

Wide Field Imaging Issues for the ATA

Ron Ekers & Geoffrey C. Bower

ABSTRACT

We consider wide field imaging issues for the Allen Telescope Array. A combination of high sensitivity, low angular resolution and large primary beam make important a number of issues for imaging with the ATA which are not typically important for other interferometers. We discuss primary and secondary gain calibration, bandpass calibration, bandwidth smearing, non-coplanar array effects and strong source noise. These introduce complexity for the online imaging backend envisioned for the ATA. Other important issues that we do not consider are mosaicing and polarization calibration. Many of these considerations point to the need for imaging simulations to determine the level of their significance.

1. Introduction

The large primary beam of the ATA introduces a number of advantages and problems for interferometric imaging. Large fields can be quickly imaged. However, care must be taken in calibration, formation of the image and deconvolution.

We assume a 350-element array of 6.1m dishes with a maximum baseline of 700 km. The array will have a resolution of $\sim 75''$ and a primary beam FWHM of $136'$ at 1.4 GHz. For a system temperature of 40 K, the sensitivity will be $250 \mu\text{Jy}$ in single polarization of a 100 MHz bandwidth in 1 minute of integration (Wright 2001). This will produce 6 mJy rms in a 200 kHz channel in the same integration time.

The rms confusion limit is $85 \mu\text{Jy}$ at 1.4 GHz and $6 \mu\text{Jy}$ at 5.0 GHz (Bower 2000). However, there will be many brighter sources in the primary beam. Below 1 mJy, the source counts are roughly Euclidean. Above 1 mJy, the source counts decline more steeply with increasing flux density. The mean brightest source in an ATA field will be 700 mJy at 1.4 GHz and 30 mJy at 5.0 GHz. Since these statistics are not Gaussian but Poisson, the maximum confusing flux will vary significantly.

We show a simulated ATA field obtained from merging 1.4 GHz NVSS images (Figure 1). The NVSS image has a beam size of $45''$ at 1.4 GHz, slightly smaller than that of the ATA. The image has an rms flux density of $500 \mu\text{Jy}$, about what would be achieved in 15 seconds for the ATA with 100 MHz of bandwidth. There are ~ 250 sources in the image above 3 mJy, which is close to

the number predicted from global source counts. The maximum flux density is 1.19 Jy and the total flux density recovered is ~ 5 Jy. Self-calibration schemes will necessarily require models that include > 100 sources to account for the majority of the flux (Figure 2). Such self-calibration may be steered using the NVSS catalog as an input although that may not be necessary since an ATA snapshot should be much higher quality than NVSS. Sources below 3 mJy will contribute $\sim 1\%$ of the total flux. Inadequate modeling of these sources may limit dynamic range to 100.

An important issue for testing of self-calibration schemes is what fraction of the flux must be accurately modeled in order to determine the gains to a certain accuracy. Naively, one assumes that the error in gains is proportional to the fraction of unmodeled flux. However, if this flux is smoothly distributed, then this will overestimate the noise.

The accuracy of self-calibration and the image dynamic range will be set by the width of the field imaged. As we show in Figure 3, the flux density in an unbiased field will be dominated by sources at a radius of HWHM or greater, even when we include the primary beam attenuation. To account for $\sim 90\%$ of the flux one must image to 1.5 HWHM. To account for $\sim 99\%$ of the flux one must image to 2.0 HWHM. This implies image sizes of 160 and 220 independent cells, respectively. With three times oversampling of cells, we require images of $\sim 512 \times 512$ pixels. In certain cases where a bright source is in the far edge of the primary beam or in sidelobes, larger maps may be necessary.

2. Primary and Secondary Gain Calibration

Primary gain calibration is typically done using an astronomical source of known and stable flux density. 3C 48, 3C 138, 3C 147 and 3C 286 are the primary gain calibrators for the VLA. NVSS images of these sources suggest that there may be substantial structure on large scales (Figure 4). Modeling of the visibilities will almost certainly be necessary, potentially including cut offs in baseline ranges.

3. Secondary Gain Calibration

Secondary gain calibration is necessary to eliminate the variable effects of the ionosphere and troposphere on signal propagation as well as variations in instrumental gain. As discussed above, self-calibration may be possible in many fields. This will be especially true at long wavelengths where the flux densities are highest and the primary beam width is largest. There is probably a cutoff frequency at which self-calibration cannot be achieved due to the absence of sources. Single source calibration will be difficult to achieve at ~ 5 GHz since the brightest source in the typical field will be ~ 30 mJy. Since the error in gains from self-calibration goes as $\sqrt{N}\sigma_b/S$, the SNR in gain for a 30 mJy source with 1 minute of integration is ~ 6 . However, the integrated flux in the field will be many times that amount. Thus, self-calibration should be applicable at frequencies

higher than 5 GHz. Spectral line observations will probably be calibrated by switching from low to high bandwidth periodically if the gain SNR is not sufficient. This places the requirement on the correlator that there are no phase jumps with bandwidth.

Very confused fields in the Galactic plane will probably require calibration in independent fields. The compact configuration of the ATA will enable longer gaps in time and larger deviations in angle between calibrators and target fields than typically allowed at other interferometers.

4. Bandpass Calibration

Accurate bandpass calibration will be crucial for detection of faint sources in HI and other lines. Extragalactic HI observations place the highest demands on the system: they require deep integrations in relatively wide bandwidth channels. A 1 hour observation with 200 kHz channel resolution will achieve a sensitivity of 0.8 mJy/beam. With a typical bright source of 700 mJy in the primary beam, bandpass calibration must be performed with a dynamic range greater than 1000. A 1 minute observation of a 4 Jy source is therefore adequate. There are approximately 100 such sources in the sky, making them readily observable.

Observing at higher redshift will introduce greater confusion and dynamic range problems. The number accounts at 843 MHz are approximately 5 times higher than at 1.4 GHz, implying that the brightest source in the primary beam will > 3 Jy. For similar observations as above, one requires bandpass calibration dynamic range on the order of 5000. This can be achieved with 25 minutes on a 4 Jy source. That is, one must spend one third of observing time doing bandpass calibration.

The bandpass must be stable on the timescale of calibration. For the low redshift HI example, one doesn't require stability beyond an hour. For the high redshift HI example, the timescale must be many hours in order for observing to be efficient.

For very long observations, the field will be confused. At 1.4 GHz, this will be for observations of 24 h or longer in 200 kHz. The confusion limit at 843 GHz will be substantially higher, requiring only ~ 1 hour observations. This confusion must be modeled.

Delay interpolation introduce bandpass fluctuations (D'Addario 2002, Figure 5). These fluctuations have a maxima of $\sim 4\%$ in the power spectrum at frequencies of $0, \pm 22$ MHz and ± 40 MHz. Performance is slightly worse at the band edge. These fluctuations vary with delay step although the shape remains similar. The delay will be tracked to an accuracy of 1 ns, leading to delay step intervals of ~ 12 s for the most distant antennas and ~ 12 min for the innermost antennas. The fluctuations will wash out over multiple delay steps allowing dynamic range greater than 100. If greater dynamic range is required, it may be necessary to model the fluctuations due to delay steps. These are completely predictable and can be reconstructed as long as the delay offsets for each signal channel are recorded. The bandpass filter shape over bandwidths < 10 MHz

will be considerably more linear than over larger bandwidths.

5. Bandwidth Smearing

Sources are smeared in a radial direction by a term proportional to the distance from the field center and $\delta\nu/\nu$, where $\delta\nu$ is the channel bandwidth and ν is the observing frequency. This has the effect of reducing sensitivity as a function of radius ξ from the field center:

$$R = \frac{\sin(\pi \frac{\delta\nu}{\nu} \frac{\xi}{\theta_b})}{\pi \frac{\delta\nu}{\nu} \frac{\xi}{\theta_b}}, \quad (1)$$

where θ_b is the primary beam size. As the argument goes to zero, R goes to zero. So, we require that

$$\frac{\delta\nu}{\nu} \ll \frac{\theta_b}{\theta_p} \sim 0.01, \quad (2)$$

where θ_p is the primary beam. Therefore, we require $\delta\nu \ll 10$ MHz for observations at 1 GHz. This places a requirement of ~ 100 channels to image the primary beam over the full 100 MHz. An accurate determination of the loss due to bandwidth can be made using the actual bandpass. In the case of imaging fields larger than the primary beam or in the case of low frequency observations, restrictions on channel width are more severe.

Bandwidth smearing will lead to errors in bandpass calibration if not addressed. Continuum sources will be smeared whereas line sources will not.

6. Non-coplanar Baselines

The combination of a curved sky and baselines which do not remain in a plane as the Earth rotates mean that the 2-dimensional FT relationship between the measured visibilities and the sky brightness distribution only holds if the following is true:

$$\pi w (\xi^2 + \eta^2) \ll 1, \quad (3)$$

where $w = \tau_g/\lambda$ is the third dimension of the visibility coordinates and ξ and η are the direction cosines of the position on the sky with respect to the phase center. TMS (1991) show that this leads to a positional error at the edge of the primary beam

$$\frac{\delta\theta}{\theta_b} = \pi \left(\frac{\theta_p}{2} \right)^2 \theta_b^{-1} \sin Z = \frac{\pi \lambda D}{4 d^2} \sin Z, \quad (4)$$

where Z is the zenith angle, D is the array diameter and d is the dish diameter. At 11.2 GHz, this term is $0.5 \sin Z$. However, at 1 GHz, the term is > 1 , even for observations close to the zenith.

There are several potential methods for addressing this error. 3-dimensional imaging will require the addition of only a few planes in the z dimension. Tessellating involves breaking the image into subplanes. The NVSS survey employed the final technique, a simple geometric correction applied after imaging.

7. Strong Source Noise

Strong sources will contribute only weakly to the system temperature of individual antennas. The gain will be ~ 150 Jy/K, implying that sources must be brighter than 1000 Jy to have an appreciable effect on the system temperature.

However, the gain of the entire array is ~ 2 K/Jy. A phased array beam in the direction of a bright source will show a substantial increase in the system temperature. Similarly but less intuitively, the noise in synthesized images in the direction of bright sources will increase. Some of this noise will also be scattered into synthesized beam sidelobes of a dirty image (Anantharamaiah *et al.* 1991). For a typical 1.4 GHz field, there will be $\sim 0.1\%$ variation in the noise in a dirty image away from bright sources. Deconvolution can remove this noise (McCullough 1993).

This noise term will primarily affect spectral line measurements in the direction of bright background sources. Noise estimates made off source will be biased. Measurements of strong source variability, continuum or line, must also take into account this error. We show the magnitude of this effect for the ATA in Figure 5.

Observations in the direction of the Galactic Center and at low frequencies in the Galactic plane will be particularly hard hit by this problem. The peak flux density at 1.4 GHz from the NVSS image of the Galactic Center is 17 Jy/beam, implying that the system temperature will double.

8. References

- Anantharamaiah, K.R., *et al.*, 1991, ASP Conf. Ser. #19, Cornwell & Perley, eds.
- Bower, G.C., 2000, ATA Memo Series #9
- D’Addario, L., 2002, ATA Memo Series #43
- McCullough, P.R., 1993, AJ, 106, 797
- Thompson, A.R., Moran, J.M. & Swenson, G.W., Jr., 1991, Interferometry and Synthesis in Radio Astronomy, Krieger Publishing Co, Florida
- Wright, M.C.H., 2001, ATA Memo Series #30

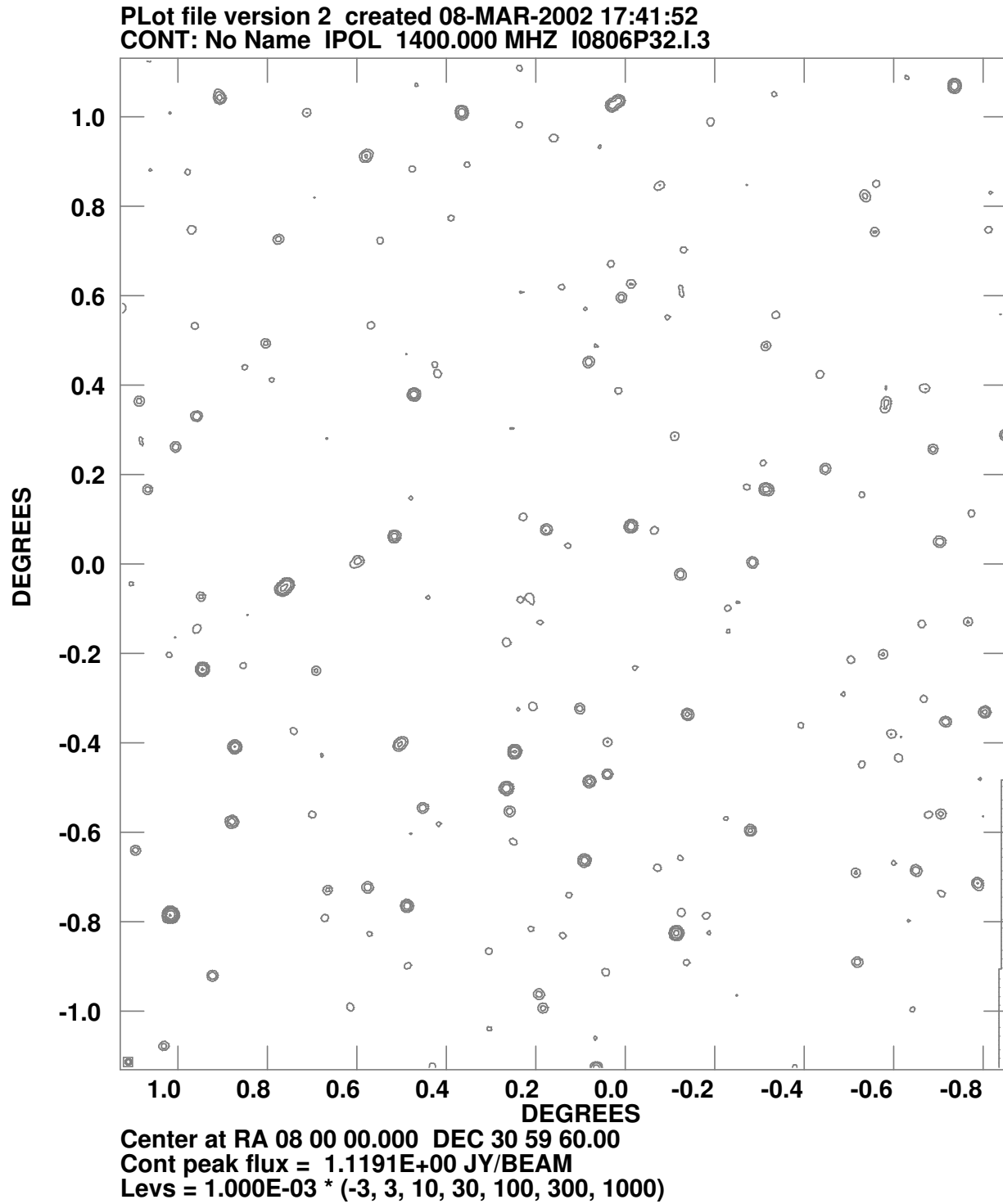


Fig. 1.— Simulated ATA field at 1.4 GHz obtained from NVSS data centered at 8h and 31^{deg}. Contours are 3, 10, 30, 100, 300 and 1000 mJy. The image rms is 500 μ Jy.

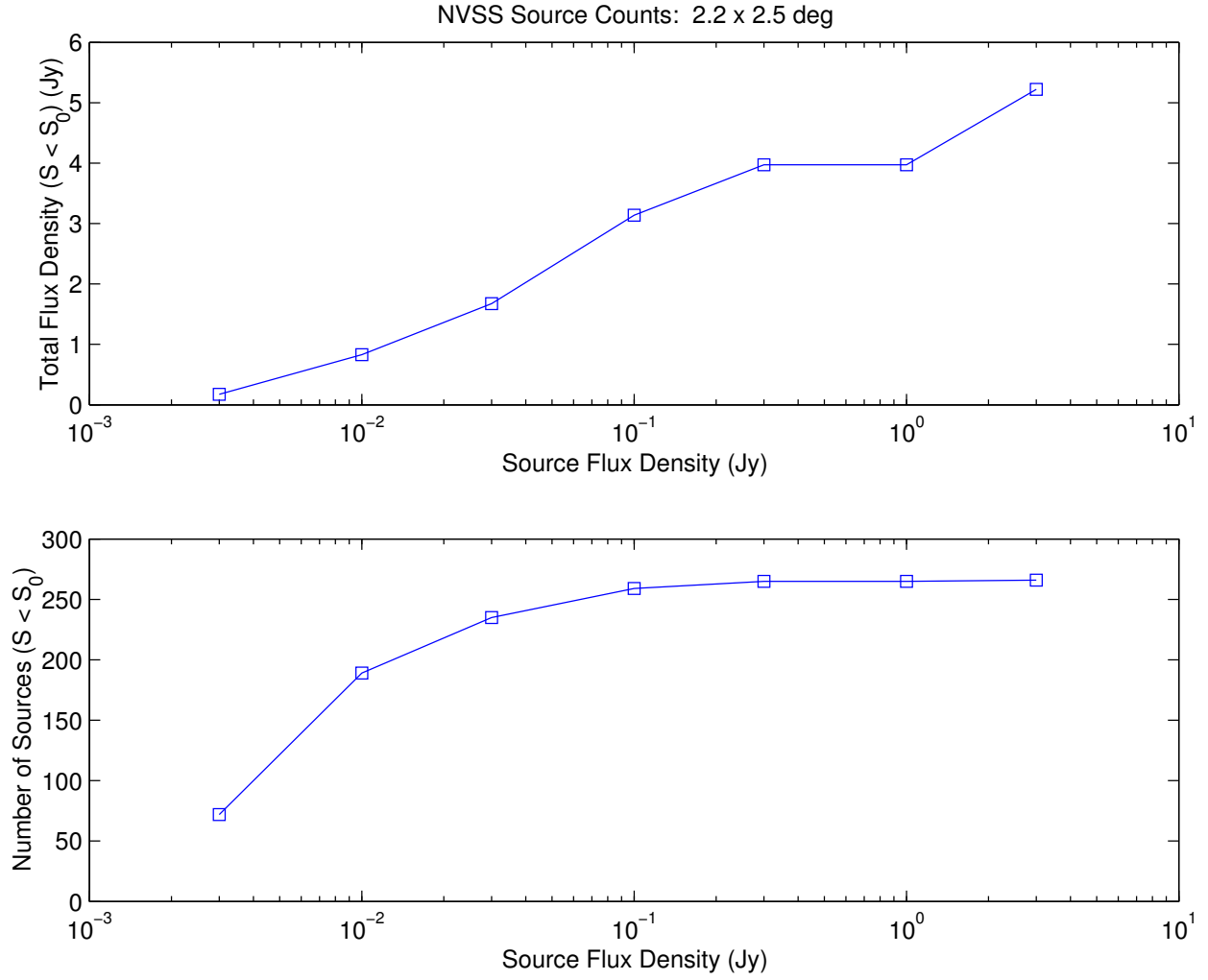


Fig. 2.— Total flux density as a function of maximum flux density for an ATA field constructed from NVSS fields (top panel). Number of sources as a function of maximum flux density for the same field (bottom panel).

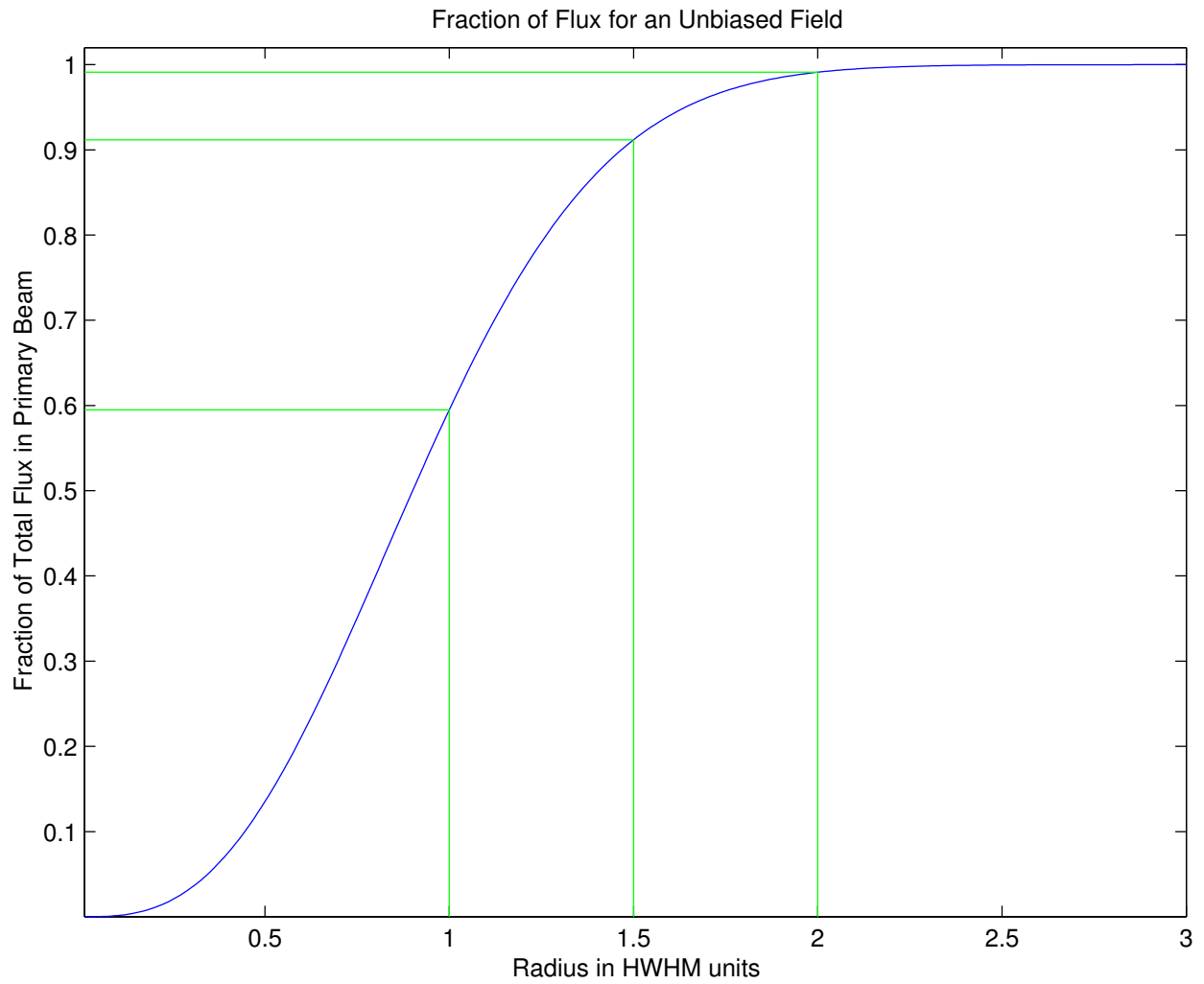


Fig. 3.— The fraction of background source flux inside a given radius of the primary beam for an unbiased field. At radii of 1, 1.5 and 2 HWHM, 59%, 91% and 99% of the flux is included, respectively.

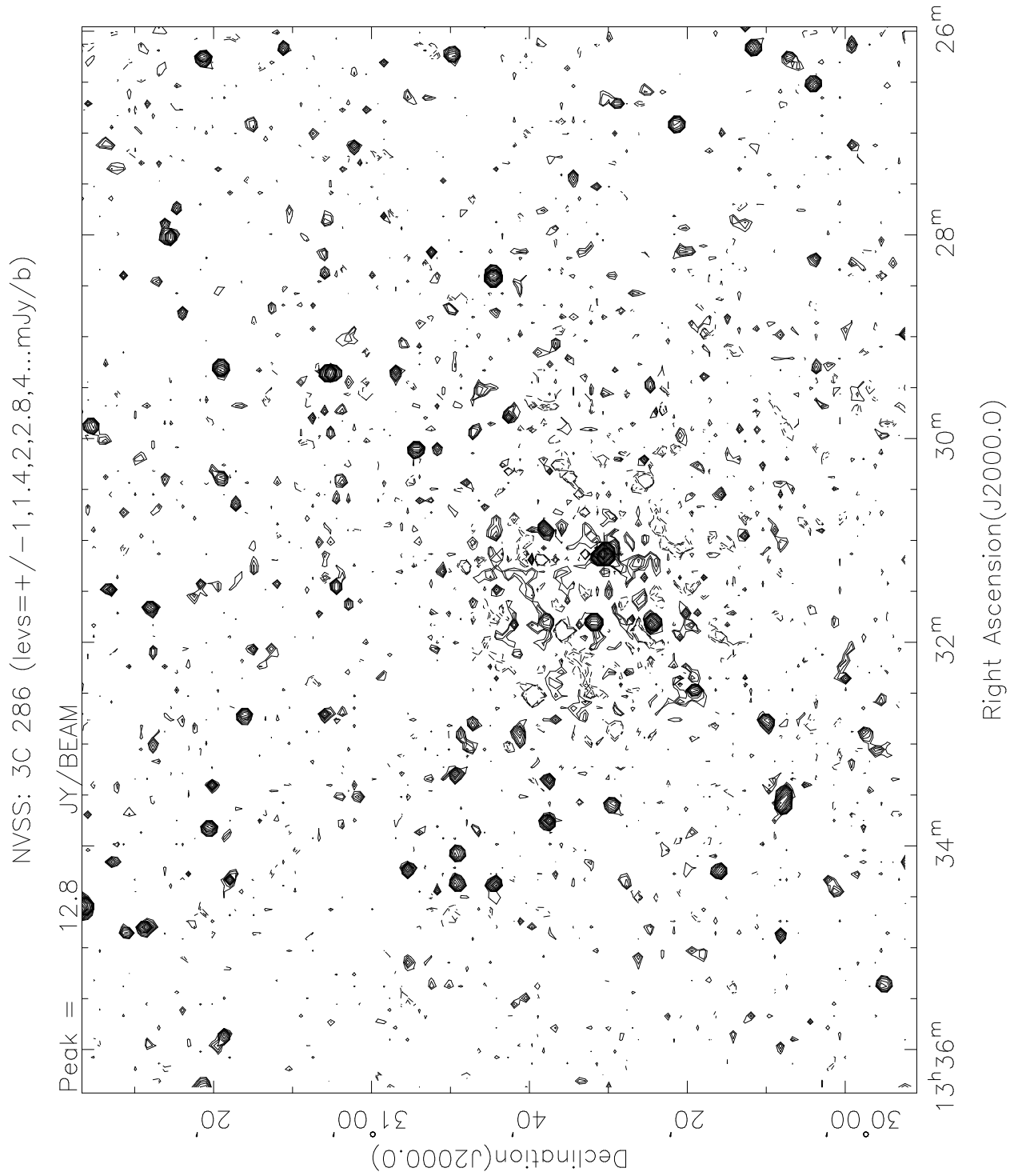


Fig. 4.— NVSS image of the region including 3C 286. There is clearly low resolution flux that is not adequately imaged.

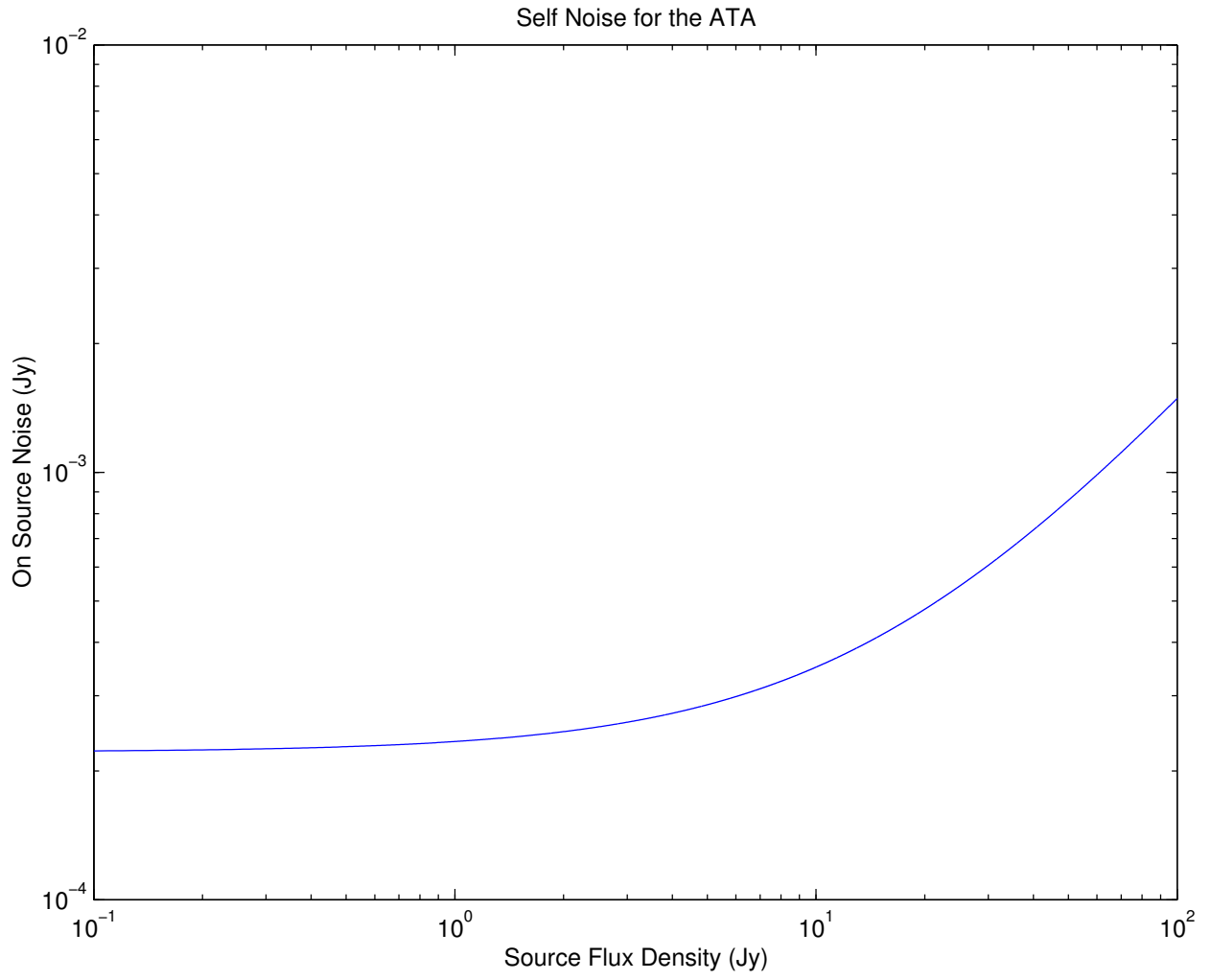


Fig. 5.— On-source self-noise calculated for the ATA as a function of source flux density.